

## The Curvature Sensitivity of a Membrane-Binding Amphipathic Helix Can Be Modulated by the Charge on a Flanking Region

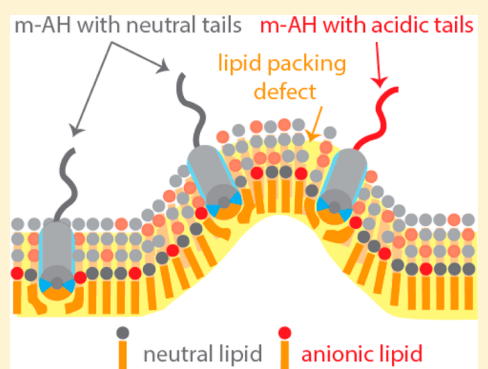
Sharon S. Y. Chong,<sup>†</sup> Svetla G. Taneva,<sup>†</sup> Joseph M. C. Lee,<sup>†,§</sup> and Rosemary B. Cornell\*,<sup>†,‡</sup>

<sup>†</sup>Department of Molecular Biology and Biochemistry, Simon Fraser University, Burnaby, British Columbia, Canada V5A 1S6

<sup>‡</sup>Department of Chemistry, Simon Fraser University, Burnaby, British Columbia, Canada V5A 1S6

### Supporting Information

**ABSTRACT:** Membrane-induced amphipathic helices (m-AH) can act as membrane curvature sensors by binding preferentially to hydrophobic lipid packing defects enriched in curved surfaces. Reliance on hydrophobicity and membrane curvature for binding is enhanced when electrostatic interactions are weak. We probed the role of modifying membrane and protein charge on the curvature sensing of two m-AH-containing proteins, CTP:phosphocholine cytidylyltransferase (CCT) and  $\alpha$ -synuclein ( $\alpha$ -syn). The m-AH domains in both proteins are flanked by disordered tails with multiple phosphoserines (CCT) or acidic residues ( $\alpha$ -syn), which we mutated to glutamate or serine to modify protein charge. Analysis of binding to vesicles of varying curvature showed that increasing the negative charge of the tail region decreased the binding strength and augmented the curvature dependence, especially for CCT. We attribute this to charge repulsion. Conversely, increasing the membrane negative charge damped the curvature dependence. Our data suggest that discrimination of curved versus flat membranes with high negative charge could be modulated by phosphorylation.



A simple way to identify an organelle is by the shape of its membrane. The endoplasmic reticulum (ER) membrane, for example, can be distinguished by its diverse curvatures, ranging from highly curved tubules to flatter cisternal structures.<sup>1</sup> Cells use such dynamic membrane landscapes to organize biochemical reactions, both spatially and temporally.<sup>2,3</sup> This implies that peripheral membrane-binding proteins have evolved ways to discriminate between flat and curved membranes. What are the membrane and protein physicochemical features that promote interactions when the membrane surface curvature is increased? This problem has received much attention.<sup>2–7</sup> A major feature of curved membrane surfaces is an increase in the size and number of lipid packing defects that expose hydrophobic binding sites for proteins.<sup>5</sup> Antonny and colleagues have proposed that the balance between the two major binding forces, electrostatics and hydrophobicity, determines the curvature sensitivity of a protein.<sup>2,3,6</sup> The weaker the electrostatics of the interaction, the greater the dependence on hydrophobicity and membrane curvature. Thus, the membrane binding of proteins with a strong curvature dependence will be predominately driven by hydrophobic mechanisms.

The best-characterized motif used by proteins to sense membrane curvature is the amphipathic helix (AH). Such structures are usually (but not always) induced by membrane binding from an ensemble of structures in the unbound form of the protein.<sup>6,8</sup> We refer to them as membrane-induced amphipathic helices (m-AH). When fully folded and membrane-bound, m-AH have a polar face exposed to the aqueous

phase and a nonpolar face that embeds into the hydrophobic core of the lipid bilayer. Bending the membrane exposes the hydrophobic membrane interior, promoting the insertion of the nonpolar face. Binding is also driven by the alleviation of lipid packing stress once the AH inserts into the defect sites.<sup>6,8–10</sup>

m-AH motifs vary greatly in features such as length, amphipathy, charge, hydrophobicity, and the positioning of charged residues in the polar face.<sup>6,8</sup> How do these features correlate with curvature sensing? The amphipathic lipid-packing sensor (ALPS) motif found in Arf-GAP, the golgin GMAP-210, Osh4p, and other proteins is a well-described m-AH that is highly curvature-dependent.<sup>6,11</sup> This m-AH motif has a strong hydrophobic face populated with bulky residues and a weak polar face rich in serine and threonine. Mutations in the m-AH Arf-Gap1 ALPS that increased the polarity of the nonpolar face diminished the hydrophobic imbalance and reduced the level of curvature sensing.<sup>11</sup> Other m-AH motifs bind equally well to curved and flat membranes, such as the AH in the antimicrobial peptide, magainin.<sup>12</sup> In contrast to the curvature-sensing m-AH motifs, these m-AH have strongly charged polar faces. Curvature-based interactions could be controlled by modulation of the membrane lipid composition, which can change the membrane surface negative charge density, hydrophobicity, or packing defects.<sup>9,13</sup> Alternatively, or in concert with membrane-based changes, curvature sensing

**Received:** October 25, 2013

**Revised:** January 6, 2014

**Published:** January 7, 2014



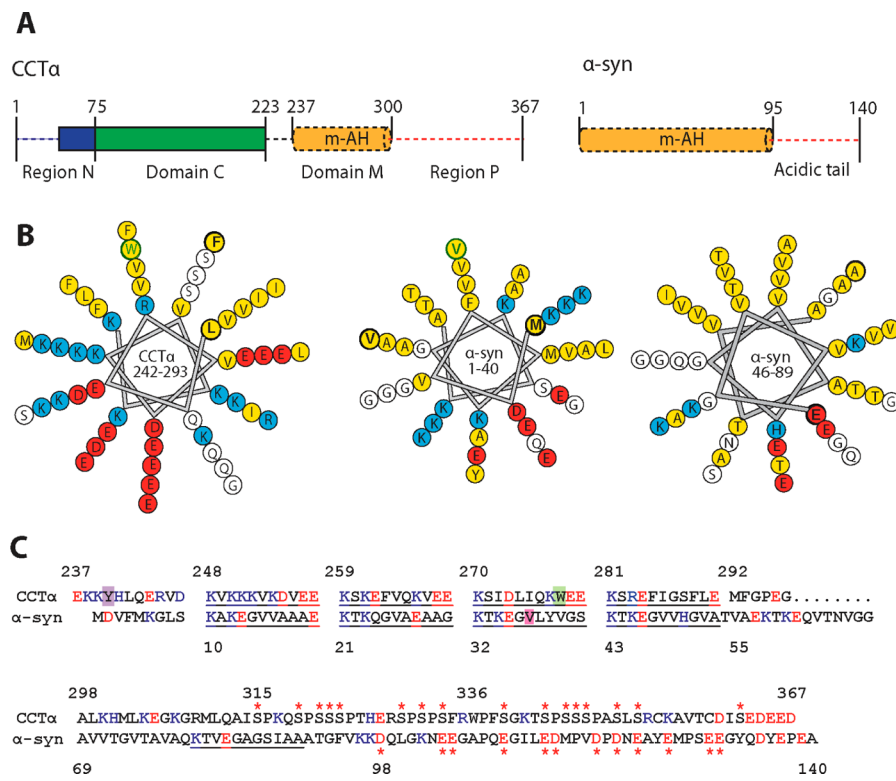


**Figure 1.** Comparison of the M+P region of CCT $\alpha$  and  $\alpha$ -synuclein. (A) CCT $\alpha$  is composed of region N, which is disordered from residue 1 to 39 (dashed blue line), a highly conserved catalytic domain (domain C, green), and an m-AH in the M domain (yellow), followed by a disordered phosphorylation (P) region (dashed red line).  $\alpha$ -Syn contains a long m-AH (yellow) followed by a highly acidic tail (dashed red line). (B) 11-3 helical wheel plots of the m-AH regions of CCT $\alpha$  and  $\alpha$ -syn. Blue indicates basic residues, red acidic residues, and yellow hydrophobic residues. The omitted segment between the two helices of  $\alpha$ -syn (residues 41–45) is nonhelical in several structural analyses.<sup>51–53</sup> The starting and ending residues are shown in bold. Sites used to monitor membrane binding, W278 in CCT and V37 in  $\alpha$ -syn, are highlighted in green. (C) Sequence alignment of  $\alpha$ -syn and CCT $\alpha$  M+P. Blue indicates basic residues and red acidic residues. 11-mer motifs are underlined. Red asterisks above the CCT sequence indicate the 16 serines that were mutated to glutamates to generate the phosphomimetic, CCT (PM). Red asterisks below the  $\alpha$ -syn sequence indicate the 12 glutamates and aspartates that were mutated to serines to create a neutralized tail ( $\alpha$ -syn12S). Y240 of CCT (purple box) was mutated to cysteine for NBD labeling (with native cysteines at positions 354 and 359 mutated to serine). W278 of CCT (green box) was used for native fluorescence measurements, in a W336F construct. The Trp fluorescence in  $\alpha$ -syn utilized an engineered Trp at V37 (pink box).

could be modulated by changing the protein electrostatics, for example, by phosphorylation. In this work, we have conducted a simple probe of the hypothesis that a reduction in the level of protein–membrane electrostatic attraction can strengthen the curvature dependence. We compare two proteins that bind membranes reversibly using very long m-AH motifs flanked by regions of variable negative charge:  $\alpha$ -synuclein ( $\alpha$ -syn) and CTP:phosphocholine cytidylyltransferase (CCT). We refer to them as being amphitropic because their functions are modulated by reversible membrane interactions.

CCT catalyzes the rate-limiting step in the synthesis of phosphatidylcholine (PC). Amphitropic regulation of CCT provides a means to coordinate the PC synthesis rate with the membrane PC content.<sup>14</sup> CCT consists of a catalytic  $\alpha/\beta$  domain<sup>15</sup> and a regulatory domain. The latter is comprised of an m-AH (domain M) followed by a carboxy-terminal phosphorylation region [region P (Figure 1A)]. Domain M transforms from a mostly disordered conformation in the CCT soluble form to an ~60-residue m-AH in response to shifts in membrane lipid composition.<sup>16</sup> These shifts include increases in the content of anionic lipids or lipids with a small headgroup relative to the hydrophobic volume, both of which are indications of a PC deficiency.<sup>8</sup> Membrane binding of domain M dissociates its autoinhibitory interaction with the catalytic domain and induces an activating conformation at the active

site.<sup>14,17–19</sup> Region P is relatively nonconserved and remains highly unstructured even in the presence of lipids.<sup>20</sup> In the CCT $\alpha$  isoform, all 16 serine residues in this region are known to be phosphorylated to some extent. Purified CCT $\alpha$  preparations feature an average of six phosphorylations<sup>20,21</sup> (Figure 1C). There is a well-established correlation between the increased level of phosphorylation and the accumulation of the soluble, inactive form of CCT.<sup>22–25</sup> Phosphorylation reduces the *in vitro* membrane binding affinity of full-length CCT $\alpha$  and CCT $\beta$ .<sup>26,27</sup>

Previous work has demonstrated that the CCT m-AH can induce membrane curvature upon binding. CCT is required for the expansion and remodeling of the nuclear envelope to generate an invaginating membrane network known as the nucleoplasmic reticulum.<sup>28,29</sup> EM analyses revealed the preferential localization of CCT $\alpha$  with highly curved nuclear invaginations (tubules) induced by a buildup of farnesylated prelamin<sup>28</sup> or by CCT overexpression and/or membrane translocation in cell nuclei.<sup>30,31</sup> A direct role for CCT in nuclear membrane remodeling was supported by *in vitro* tubulation of lipid vesicles.<sup>31,32</sup> Curvature induction in cells and *in vitro* was shown to be mediated by the CCT m-AH.<sup>30,32</sup> An EM analysis showed that the conversion of vesicles into highly curved tubes involved growth of the tubule from a bud, suggesting a cooperative process whereby CCT-induced local

curvature serves as a target for binding of additional CCT.<sup>32</sup> This provided the first hint of a curvature-dependent membrane binding process.

$\alpha$ -Syn is an amphitropic protein associated with neuronal synaptic vesicles that are  $\sim$ 50 nm in diameter.<sup>33</sup> Its function is still under intense investigation but has been implicated in stabilizing SNARE complexes that mediate fusion of the synaptic vesicle with the plasma membrane.<sup>34</sup> Its misfolding into fibrillar oligomers is linked to neurotoxicity and Parkinson's disease.<sup>35–39</sup> Like CCT,  $\alpha$ -syn contains a continuous  $\sim$ 80–90-residue AH when membrane-bound<sup>40</sup> (Figure 1A). The m-AH of  $\alpha$ -syn shares a novel 11-mer sequence motif with the CCT domain M<sup>18,41</sup> (Figure 1C). Like CCT, the m-AH in  $\alpha$ -syn transitions from a disordered structure to a fully folded helix when presented with membranes enriched in acidic lipids or packing defects.<sup>42,43</sup> Its m-AH is followed by an unstructured, highly acidic tail (15 aspartates and glutamates), resembling the phosphorylated state of the CCT tail. In addition, the C-terminal region of  $\alpha$ -syn can be phosphorylated at Tyr 125, 133, and 136, and on Ser 129,<sup>44</sup> further increasing the charge of its tail. Many functions for the acidic tail have been suggested,<sup>45</sup> including serving as the contact site for proteins such as the v-SNARE, synaptobrevin.<sup>34</sup> Membrane binding of  $\alpha$ -syn is similarly driven by a mixture of electrostatic attraction to anionic lipids and a hydrophobic component that favors binding to highly curved vesicles.<sup>46–48</sup>  $\alpha$ -Syn not only senses curvature but also is curvature-inducing.<sup>32,49,50</sup>

Despite the similarities between the m-AH motifs of CCT and  $\alpha$ -syn, these two m-AH motifs differ in the hydrophobicity of their nonpolar faces. Whereas the nonpolar face of the CCT m-AH is rich in bulky and aromatic amino acids, that of  $\alpha$ -syn features short aliphatic residues such as valine, alanine, and even glycine (Figure 1B). These differences led to the prediction that the two proteins might show differences in curvature sensitivity and in their responses to a change in protein electrostatics.

## EXPERIMENTAL PROCEDURES

**Materials.** Egg PC and egg PG were purchased from Avanti Polar Lipids Inc. The concentrations of the phospholipid chloroform stocks were determined by a phosphorus assay.<sup>54</sup> Ni-NTA agarose was from Qiagen, and thrombin protease was from Amersham Biosciences. The Spectra/Por 7 dialysis membrane (10 kDa molecular mass cutoff) was purchased from Spectrum Laboratories. Amicon Ultra-4 centrifugal filters were from Millipore. Polycarbonate membranes used in extrusion of vesicles were purchased from Avestin Inc. *N,N'*-Dimethyl-*N*-(iodoacetyl)-*N*'-(7-nitrobenz-2-oxa-1,3-diazol-4-yl)ethylenediamine (termed iodoacetyl NBD-amide) was purchased from Invitrogen. Other reagents were from Sigma-Aldrich.

**Preparation of Plasmids for Transfection.** The unphosphorylated CCT (UP) proteins encompassed residues 237–367 of rat CCT $\alpha$ , which include the M domain and the P region (Figure 1A,C). The phosphomimic [CCT (PM)] protein had 16 serine to glutamate substitutions between residues 315 and 367 at the positions denoted in Figure 1C. We used wild-type human  $\alpha$ -syn as well as an  $\alpha$ -syn construct in which 12 acidic glutamates and aspartates between residues 98 and 140 were mutated to serines ( $\alpha$ -syn12S) as shown in Figure 1C. The construction of pET14b plasmids containing wild-type and PM versions of the CCT M+P domains and wild-type  $\alpha$ -syn was described previously.<sup>32</sup> pET14b- $\alpha$ -syn12S was

prepared by gene synthesis. Double-stranded DNA encoding  $\alpha$ -syn with AGC mutations to create serine at the 12 sites denoted above was synthesized (Eurofin Operon) with 5' NdeI and 3' XhoI restriction sites. The digested synthetic gene was ligated into the NdeI and XhoI sites of similarly digested pET14b.

For tryptophan fluorescence analysis, we generated variants with a single Trp within the m-AH regions of CCT and  $\alpha$ -syn. CCT has a native Trp at position 278 in the hydrophobic face of its m-AH. A second Trp at position 336 in the P region was replaced with a Phe using QuikChange site-directed mutagenesis with pET14b-CCT M+P (UP) and pET14b-CCT M+P (PM) as templates and mutagenic primers complementary to the targeted sequence. Because  $\alpha$ -syn has no native Trp, we engineered a Trp at position 37 (replacing Val) in the hydrophobic face of its m-AH using QuikChange mutagenesis, mutagenic primers, and pET14b- $\alpha$ -Syn or pET14b- $\alpha$ -syn12S as a template.

For NBD fluorescence analysis, we generated single-cysteine variants of CCT M+P. We replaced the two naturally occurring cysteines located in the P region (positions 354 and 359 in full-length CCT $\alpha$ ) with serine and engineered a cysteine in the hydrophobic face of domain M at position 240 of full-length CCT $\alpha$  in place of a tyrosine. The Y240C mutation corresponds to residue 8 in our CCT M+P proteins, which had four N-terminal residues (GSHM) from the linker to the thrombin cleavage site. These mutations were generated by QuikChange using pET14b-CCT M+P (UP) or (PM) as templates. The fidelity of all proteins generated by QuikChange mutagenesis was checked by sequencing of both strands.

**Expression and Purification of CCT M+P and  $\alpha$ -Syn.** The pET14b-CCT M+P and  $\alpha$ -syn constructs permitted expression in the *Escherichia coli* Rosetta strain as His<sub>6</sub>-tagged proteins with thrombin cut sites. The CCT M+P proteins were induced with IPTG for 2 h at 20 °C and the  $\alpha$ -synuclein proteins for 3 h at 37 °C, and the cells were lysed by sonication. Other steps of the expression, purification, and His<sub>6</sub> tag cleavage followed described protocols.<sup>32</sup> The concentrations of purified proteins were determined by Bradford analysis<sup>55</sup> and by the absorbance at 280 nm and molar extinction coefficients. Purified proteins were stored at  $-80$  °C in PBS (pH 7.4), 0.1 mM octyl glucoside, and 2 mM DTT.

**Labeling of CCT M+P Proteins for NBD Fluorescence Measurements.** NBD was conjugated via a stable thioether bond to the engineered cysteine at residue 240 (Y240C). The protein in PBS and 1 mM DTT was adjusted to 0.3 M NaCl and 6 mM OG to reduce the aggregation propensity. The His<sub>6</sub> tag was completely cleaved with 1 unit of thrombin/50  $\mu$ g of peptide at room temperature for 1 h with rotation. Iodoacetyl NBD-amide was prepared in DMSO at  $\sim$ 20 mM, based on the absorbance at 480 nm. The NBD was added to the digested proteins to a final concentration of 2 mM, and a 2-fold molar excess over the sum of CCT(Y240C) and DTT. DMSO was  $<5$  % of the volume. After 1 h at room temperature in the dark, octyl glucoside, free NBD and NBD–DTT conjugates, and His tags were removed via dialysis at room temperature for 4 h with one buffer change and then overnight in the dark. The dialysis buffer consisted of PBS and 0.14 M NaCl (pH 7.4). The stoichiometry of labeling was  $\sim$ 1:1 (NBD:protein molar ratio), measured via the absorbance at 480 nm for NBD and 280 nm for the protein. The protein concentration was verified with the Bradford assay,<sup>55</sup> and labeling was confirmed by visualization of fluorescent bands separated by 12% sodium dodecyl sulfate–

polyacrylamide gel electrophoresis using a Typhoon Variable Mode Imager (Amersham Biosciences). The NBD-labeled peptides were stored in the dark at  $-80^{\circ}\text{C}$ .

**Phospholipid Vesicle Preparation.** All vesicles used in these experiments were composed of egg PC and egg PG. SUVs were prepared by sonication on ice using a micro probe (Branson Sonifier 450) as described previously.<sup>56</sup> LUVs were prepared by extrusion of multilamellar vesicles at room temperature<sup>32</sup> using polycarbonate membranes with pore sizes of 30, 100, 200, and 400 nm. Vesicle size was determined by dynamic light scattering as described previously<sup>57</sup> and electron microscopy of negatively stained samples.<sup>32</sup> The diameters of the vesicles were as follows: 47 nm for SUVs and 85, 112, and 144 nm for vesicles extruded through 30, 100, and 200 nm pore filters, respectively. The polydispersity of the 400 nm extruded vesicles was very high; thus, the level of confidence in the mean diameter we obtained (155 nm) was low. We used the mean size reported for these in the literature,  $274 \pm 77$  nm.<sup>58-61</sup>

**Circular Dichroism (CD) and Deconvolution.** The proteins (5  $\mu\text{M}$ ) in dilute PBS (ionic strength of 15 mM) were mixed with varying concentrations of lipid vesicles at  $25^{\circ}\text{C}$  and incubated for 5 min. Spectra recorded after incubation of  $\alpha$ -syn with PC/PG SUVs for 5 or 120 min were nearly identical, indicating equilibration of the binding within 5 min (data not shown). The buffer contained a low salt concentration to reduce the level of interference from light scattering. CD spectra were recorded using a Jasco-J-810 spectropolarimeter in a 0.1 cm path-length cuvette at a scanning rate of 100 nm/min and a bandwidth of 1 nm. Two scans were averaged per spectrum. All spectra were smoothed, corrected for the corresponding background (buffer with or without vesicles), and converted to residue molar ellipticity (deg  $\text{cm}^2/\text{dmol}$ ). The secondary structure content was determined using the CDPro package and protein reference set #7, which includes 43 soluble and five denatured proteins.<sup>62</sup>

**NBD Fluorescence Measurements and Binding Analysis.** The proteins (0.1  $\mu\text{M}$ ) in dilute PBS (ionic strength of 115 mM) were mixed with a range of vesicle concentrations and incubated for  $\sim 5$  min at  $20^{\circ}\text{C}$ . Samples were placed in a 10 mm quartz cuvette, and spectra were recorded using a Varian Cary Eclipse spectrofluorometer with excitation at 478 nm and an emission scan from 500 to 650 nm. Excitation and emission slits were set to 10 nm; the PMT voltage was 925 V. Six scans were averaged, and the resulting spectra were smoothed and corrected for the corresponding background (buffer with or without vesicles). The average wavelength of maximal intensity for unbound CCT was 550 nm. In the presence of saturating lipid concentrations, this peak wavelength blue-shifted to 533 nm. We plotted the fluorescence intensity at 533 nm for each spectra versus  $\log[\text{accessible lipid}]$ . The accessible lipid is 60% of the total lipid concentration for SUVs and 50% for LUVs. The plots of fluorescence intensity at 533 nm versus  $\log[\text{accessible lipid}]$  were normalized to create binding curves using the following equation:

$$\% \text{ bound} = (F - F_0) / (F_{100} - F_0) \times 100\% \quad (1)$$

where  $F$  is the intensity at 533 nm ( $I_{533}$ ),  $F_0$  is the  $I_{533}$  in the absence of lipids, and  $F_{100}$  is the  $I_{533}$  at lipid saturation. The % bound curves were fit to the equation

$$\% \text{ bound} = (K_p[\text{L}]) / (1 + K_p[\text{L}]) \times 100\% \quad (2)$$

where  $[\text{L}]$  is the accessible lipid concentration and  $K_p$  is the apparent molar partition coefficient, defined as  $K_p = [\text{P}_b]/[\text{P}_f][\text{L}]$ , where  $[\text{P}_b]$  and  $[\text{P}_f]$  are the concentrations of the bound and free protein, respectively, and  $[\text{L}]$  is the concentration of the accessible lipid.<sup>63</sup> This analysis assumes a two-state conversion between free and bound protein, which is supported by the isosbestic points in the spectra of Figures 2A and 5A and Figure S1 of the Supporting Information. From these plots, we obtained the accessible lipid concentration at 50% bound ( $\text{EC}_{50}$ ) to calculate the apparent  $K_p$  values using the equation  $K_p = 1/\text{EC}_{50}$ .

### Tryptophan Fluorescence Measurements and Binding Analysis.

The proteins (1  $\mu\text{M}$ ) in dilute PBS (ionic strength of 115 mM unless noted) were mixed with lipids, and spectra were recorded, smoothed, and corrected as described above. Spectra acquired after incubation of  $\alpha$ -syn for 5 or 15 min with 274 nm vesicles (30 mol % PG) were nearly identical, indicating the equilibration of binding within 5 min (data not shown). Excitation was at 280 nm, and the emission scan was from 300 to 400 nm. Excitation and emission slits were set to 10 and 5 nm, respectively. The average wavelength of maximal intensity for unbound CCT and  $\alpha$ -syn was 350 nm. In the presence of saturating lipids, the peak wavelength blue-shifted to 325 nm. We plotted the fluorescence ratio (325 nm/350 nm) for each spectra versus  $\log[\text{accessible lipid}]$ . The plots of fluorescence ratio versus  $\log[\text{accessible lipid}]$  were normalized to create binding curves using eq 1 where  $F = I_{325}/I_{350}$ . Apparent  $K_p$  values were obtained using eq 2.

### Assessment of $K_p$ Values for Strongly Binding Proteins.

As discussed previously,<sup>63-65</sup> partitioning analyses require that the membrane surface area not be limiting. Previous analyses have determined that one CCT or one  $\alpha$ -syn m-AH requires  $\sim 25$  lipids for solvation on the membrane;<sup>32,46</sup> thus, we used the following equation to estimate the excess lipid available when 50% of the protein is bound:

$$[\text{excess lipid}] = [\text{EC}_{50}] - 25(0.5[\text{P}_t]) \quad (3)$$

where  $[\text{P}_t]$  is the total protein concentration and  $\text{EC}_{50}$ , the accessible lipid at 50% bound, is obtained from the binding curve. The term  $25(0.5[\text{P}_t])$  is the concentration of lipid in complex with the bound m-AH that is unavailable for binding additional protein. If there was no excess residual lipid at  $\text{EC}_{50}$ , the  $K_p$  values were deemed to be underestimated. Unless noted, we have reported apparent  $K_p$  values representing systems in which there was excess lipid at  $\text{EC}_{50}$ . The excess available lipid represents the concentration of free lipid at 50% saturation; thus, we also report  $K_p$  estimates ( $1/[\text{excess lipid}]$ ) in Tables 1 and 2.

## RESULTS

**The Curvature Sensitivity of the m-AH Is Modulated by the Charge of Its Flanking Region.** We used bacterially expressed, nonphosphorylated  $\alpha$ -syn and CCT regulatory domains. The CCT constructs were composed of the M and P regions in unphosphorylated [CCT (UP)] and phosphomimetic [CCT (PM)] forms. CCT (PM) is a variant with all 16 phosphoserine sites substituted with glutamates. It has been studied in the context of the full-length enzyme, showing a reduced level of membrane partitioning,<sup>23</sup> like hyperphosphorylated CCT.<sup>24</sup> Initially, we examined the vesicle size dependence of the interaction of CCT M+P proteins and  $\alpha$ -syn using circular dichroism (CD) to monitor changes in secondary structure coincident with binding. CCT (UP), CCT (PM), or

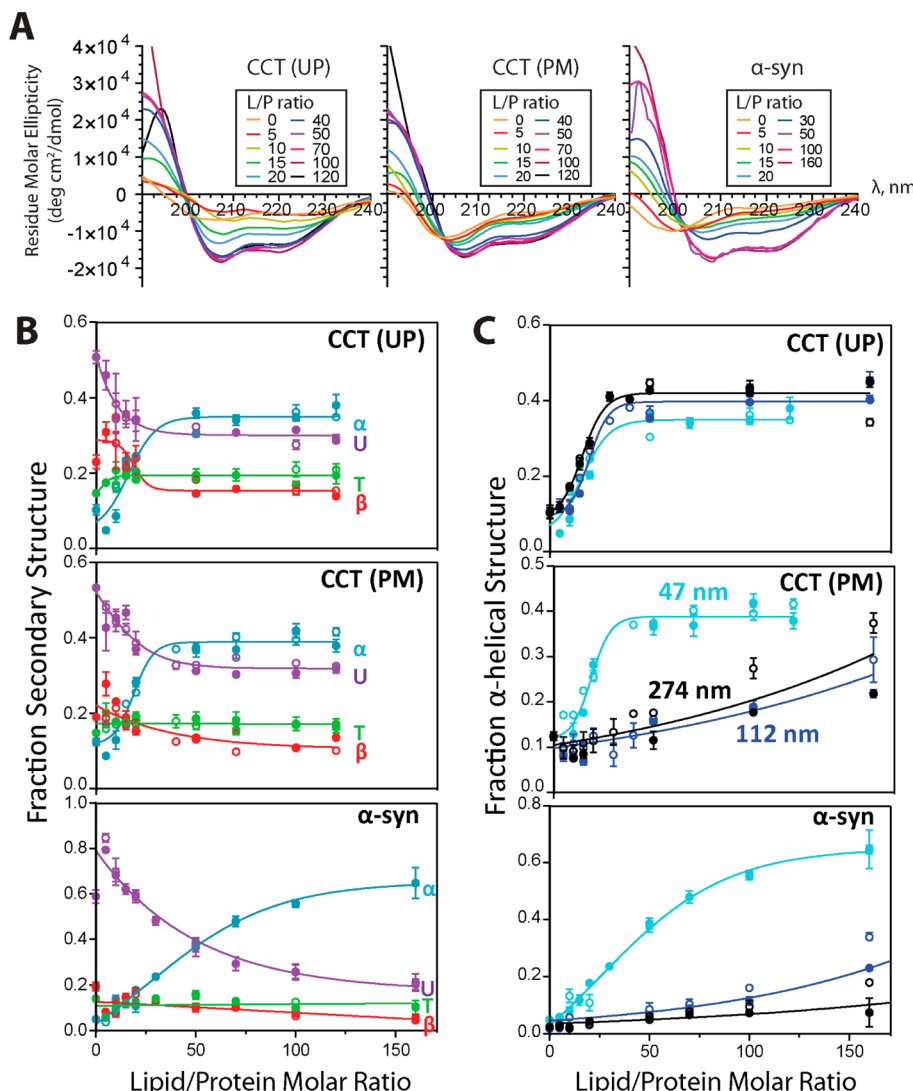


**Figure 2.** Curvature dependence of CCT and  $\alpha$ -syn probed by CD. (A) Sample CD spectral set of CCT (UP), CCT (PM), and  $\alpha$ -syn. Titration with 47 nm diameter SUVs composed of 30 mol % PG at an ionic strength of 15 mM. (B) Transition from unordered structure to  $\alpha$ -helices with an increase in lipid concentration. Spectra shown in panel A were deconvoluted to generate fractional secondary structure:  $\alpha$ -helical (blue), unordered (purple), turn (green), and  $\beta$ -strand (red). (C) CCT (PM) and  $\alpha$ -syn are more curvature-dependent than CCT (UP). Panels show the fraction of helical structure upon titration with 47 nm (light blue), 112 nm (dark blue), or 274 nm (black) vesicles composed of 30 mol % PG in 15 mM ionic strength buffer. The empty and filled symbols represent data from two independent trials. Error bars represent means  $\pm$  the standard deviation of the fractional secondary structure content deconvoluted using the three programs, SELCON, CONTINLL, and CDSSTR, within the CDPPro package.

$\alpha$ -syn was titrated with SUVs and LUVs composed of 30 mol % egg PG, whose diameters were determined by light scattering and EM. The balance lipid was egg PC in these and all other vesicles. This represents the high end of physiological anionic lipid content.<sup>66</sup> Synaptic vesicle and plasma membranes, for example, have  $\sim$ 15% anionic lipid that is distributed asymmetrically in the cytoplasmic leaflet.<sup>67</sup> PG is routinely used as a model for an anionic lipid when a membrane-binding protein (including CCT and  $\alpha$ -syn) primarily recognizes lipid charge and not the specific chemistry of the headgroup. Representative titrations with vesicles 47 nm in diameter are shown for CCT (UP), CCT (PM), and  $\alpha$ -syn in Figure 2A. The m-AH regions in CCT and  $\alpha$ -syn comprise  $\sim$ 0.44 and 0.67 of the total protein sequences, respectively. Deconvolution of CD spectra indicated that the m-AH regions of the CCTs and  $\alpha$ -syn transform from a mixture of predominantly disordered and  $\beta$ -strand conformations into nearly fully folded helical conformations in the presence of vesicles (Figure 2B). Thus, all of the protein species

from the ensemble of unbound conformations participate in the membrane binding reaction. Plots of the change in helical content versus L/P molar ratio (Figure 2C) indicated binding affinity decreased in the following order: CCT (UP)  $>$  CCT (PM)  $>$   $\alpha$ -syn. This is in keeping with previous analyses<sup>32</sup> and in agreement with the notion that repulsive charge adjacent to the m-AH can weaken affinity.<sup>26,27</sup> CCT (PM) and  $\alpha$ -syn showed a significant difference in binding to large and small vesicles, whereas CCT (UP) showed very little selectivity with respect to size (Figure 2C). Thus, it appeared that the m-AH segments flanked by acidic tails were curvature-sensitive but the m-AH segments flanked by neutral tails were not.

The CD data were acquired at a low (nonphysiological) ionic strength to reduce light scattering from large vesicles. In addition, we were concerned that the results for the strongly binding CCT (UP) may have been complicated by the limited membrane surface at low lipid concentrations. To avoid these problems and to obtain reliable partitioning coefficients, we

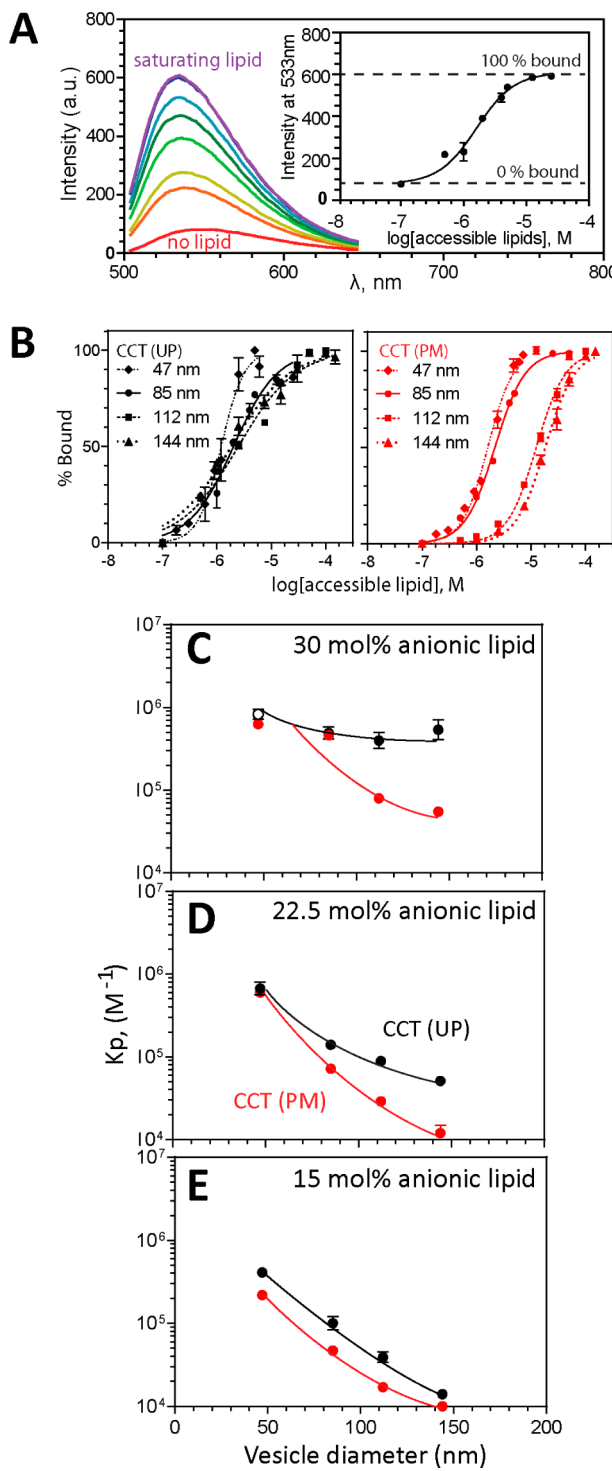


**Figure 3.** Curvature dependence of CCT (UP) and CCT (PM) probed by NBD fluorescence. (A) The fluorescence of NBD-labeled CCT shows a blue-shift and increase in intensity upon titration of 0.1  $\mu$ M CCT (UP) with 85 nm LUVs (30 mol % PG, ionic strength of 115 mM). Red to fuchsia indicates a lipid/protein molar ratio from 0 to 8000. The inset shows the corresponding lipid binding curve for this spectral set and its replicate. The intensity at 533 nm in the absence of lipid was set to 0% bound, and  $I_{533}$  at saturating lipid concentrations was set to 100% bound. (B) Binding curves show that CCT (PM) is more curvature-sensitive than CCT (UP). Vesicles were composed of 30 mol % PG, and the ionic strength was 115 mM. Black curves are for CCT (UP) and red curves for CCT (PM). Data were fit to eq 2 using GraphPad Prism version 5.0. All binding curves made good fits to this

**Figure 3. continued**

expression for a hyperbolic curve. The  $R^2$  values for the fits are listed in Tables 1 and 2. The binding curves are displayed as a function of  $\log[L]$  to facilitate visualization. (C–E) Curvature sensing of CCT can be modulated by both protein and membrane electrostatics.  $K_p$  values were determined from binding curves shown in panel B.  $K_p = 1/EC_{50}$ . Each data point is the average partition coefficient ( $K_p$ )  $\pm$  95% confidence interval for two independent binding analyses. Curves are to facilitate viewing only. The data point in the empty black circle (panel C) represents a  $K_p$  value that is likely underestimated, as there was no excess lipid present at  $EC_{50}$ . See Experimental Procedures and Table 1.

monitored the binding of the CCT M+P proteins with a more sensitive method using an extrinsic fluorescence probe. NBD was conjugated via a stable thioether bond to an engineered cysteine at position 240 (Y240C). Because NBD has a structure similar to that of tryptophan, it should not interfere significantly with membrane binding. NBD absorbs and emits in the visible spectrum where light scattering interference by large vesicles is low. Its fluorescence can blue-shift  $\sim$ 15 nm and show an enhanced quantum yield upon relocation to a hydrophobic environment.<sup>68</sup> This method allowed us to work with very low (0.1  $\mu$ M) protein concentrations and a physiological ionic strength.

Figure 3A shows a representative titration of CCT (UP) with 85 nm LUVs (30 mol % PG). We monitored membrane binding via the increase in intensity at  $\sim$ 533 nm, which is the emission wavelength representing the fully bound NBD-labeled proteins. A set of normalized binding curves for the CCTs with 30 mol % PG vesicles is shown in Figure 3B. From these curves, we extracted apparent  $K_p$  values from the accessible lipid concentration at 50% bound peptide (Figure 3C–E). The results for trials with 30 mol % PG (Figure 3C) revealed a difference in the curvature sensing of CCT (UP) versus CCT (PM), in agreement with the CD results (Figure 2C). Partitioning of CCT (UP) was independent of size between diameters of 85 and 140 nm, whereas CCT (PM) partitioning increased an order of magnitude from large to smaller vesicles. Introducing negative charges into the region flanking the m-AH weakened the binding to 144 nm diameter vesicles by  $\geq$ 10-fold but had little influence on the binding strength for  $\leq$ 85 nm diameter vesicles (Figure 3C). These results support the notion that curvature dependence is augmented by a negatively charged tail flanking the m-AH.

**Curvature Sensitivity of CCT (UP) Is Influenced by the Membrane Charge.** Vesicles with 30% anionic lipid have a strong electrostatic surface potential that could mask the impact of changes in curvature-induced membrane hydrophobicity. This might explain the apparent curvature insensitivity of CCT (UP). If strong electrostatic interaction is the basis for the curvature-independent binding, then the reduction in membrane charge should generate curvature dependence. The data in panels D and E of Figure 3, showing the partitioning into vesicles composed of 22.5 or 15 mol % PG, indicate that this is indeed the case. The binding of CCT (UP) was  $>$ 10-fold weaker with the flatter, larger vesicles than with the smaller curved vesicles. The  $K_p$  values are listed in Table 1. With vesicles containing 15 mol % PG, the size dependence for binding was nearly the same for both CCT proteins. These results indicate that membrane charge is a factor influencing curvature dependence for the CCT with an uncharged tail. On

Table 1. Apparent Partition Coefficients ( $K_p$ )<sup>a</sup> for CCT (UP) and CCT (PM)

PG (mol %)	vesicle diameter (nm)	CCT (UP)			CCT (PM)		
		apparent $K_p$ ( $\times 10^3$ M $^{-1}$ )	$R^2$	$K_p$ estimate ( $\times 10^3$ M $^{-1}$ )	apparent $K_p$ ( $\times 10^3$ M $^{-1}$ )	$R^2$	$K_p$ estimate ( $\times 10^3$ M $^{-1}$ )
30	47	830 $\pm$ 120	0.960	no excess L <sup>b</sup>	630 $\pm$ 50	0.988	2900
	85	490 $\pm$ 90	0.968	1300	460 $\pm$ 40	0.993	1100
	112	400 $\pm$ 100	0.975	820	80 $\pm$ 8	0.992	89
	144	540 $\pm$ 170	0.962	1700	55 $\pm$ 5	0.992	60
22.5	47	670 $\pm$ 130	0.968	4100	600 $\pm$ 63	0.985	2300
	85	140 $\pm$ 20	0.982	170	72 $\pm$ 6	0.986	80
	112	89 $\pm$ 7	0.995	100	29 $\pm$ 4	0.984	30
	144	51 $\pm$ 4	0.993	54	12 $\pm$ 3	0.979	12
15	47	410 $\pm$ 50	0.992	830	220 $\pm$ 30	0.918	300
	85	100 $\pm$ 20	0.978	120	47 $\pm$ 5	0.987	50
	112	39 $\pm$ 6	0.993	40	17 $\pm$ 2	0.988	17
	144	14 $\pm$ 2	0.989	15	10 $\pm$ 1	0.975	10

<sup>a</sup>Apparent partition coefficients ( $K_p$ ) equal  $1/EC_{50}$ , as derived from binding curves and eq 2. Curves were fit using GraphPad Prism version 5.0. Errors are  $\pm 95\%$  confidence intervals for at least two independent binding analyses;  $R^2$  values are taken from a curve fit to eq 2.  $K_p$  estimations were based on  $1/[excess\ lipid]$  as described in eq 3 of Experimental Procedures. <sup>b</sup>The solution to eq 3 was a negative value.

Table 2. Apparent Partition Coefficients ( $K_p$ )<sup>a</sup> for  $\alpha$ -Syn and  $\alpha$ -Syn12S

PG (mol %)	vesicle diameter (nm)	$\alpha$ -syn12S			$\alpha$ -syn		
		apparent $K_p$ ( $\times 10^3$ M $^{-1}$ )	$R^2$	$K_p$ estimate ( $\times 10^3$ M $^{-1}$ )	apparent $K_p$ ( $\times 10^3$ M $^{-1}$ )	$R^2$	$K_p$ estimate ( $\times 10^3$ M $^{-1}$ )
30	47	86 $\pm$ 21	0.955	no excess L <sup>b</sup>	78 $\pm$ 15	0.957	no excess L <sup>b</sup>
	85	40 $\pm$ 8	0.959	79	7.0 $\pm$ 2.0	0.923	7.9
	112	22 $\pm$ 3	0.981	31	6.8 $\pm$ 0.8	0.983	7.4
	144	12 $\pm$ 2	0.988	14	2.3 $\pm$ 0.2	0.992	2.4
	274	12 $\pm$ 2	0.986	14	3.0 $\pm$ 0.5	0.955	3.1

<sup>a</sup>Apparent partition coefficients were obtained as described in footnote <sup>a</sup> of Table 1. <sup>b</sup>The solution to eq 3 was a negative value.

the other hand, the partitioning of CCT (PM), with its electrically repulsive tail, showed curvature dependence regardless of the membrane charge.

The results of varying the charge of the protein or the membrane suggested that curvature sensitivity is enhanced by decreasing the electrostatic attraction. To show that introduction of repulsive negative charges adjacent to the net positively charged CCT m-AH reduces the electrostatic component of binding, we compared binding of CCT (UP) and CCT (PM) to 30 mol % PG vesicles as a function of the medium ionic strength (Figure 4) using intrinsic Trp fluorescence. The data show weak partitioning for CCT (PM) that is nearly independent of ionic strength but partitioning for CCT (UP) that is strongly ionic strength-dependent. Thus, the binding of CCT (UP) with a neutral tail is affected by changes in electrostatics, whereas that of CCT (PM) is affected much less so. These data are consistent with a stronger reliance on hydrophobic interactions for CCT (PM).

**$\alpha$ -Synuclein Curvature-Dependent Binding Is Less Sensitive to Electrostatic Modulation.** To determine whether charge repulsion adjacent to an m-AH could be a general mechanism augmenting membrane curvature sensitivity, we performed parallel experiments with  $\alpha$ -syn. For these experiments, we compared “wild-type”  $\alpha$ -syn possessing the highly acidic tail with an  $\alpha$ -syn protein that has 12 glutamates and aspartates in the tail region (residues 95–140) mutated to neutral serines [ $\alpha$ -syn12S (Figure 1C)]. The latter protein is an analogue of CCT (UP). The substitution of the 12 acidic residues with serine did not interfere with the coil to helix transition for the m-AH of  $\alpha$ -syn (Figure S1 of the Supporting

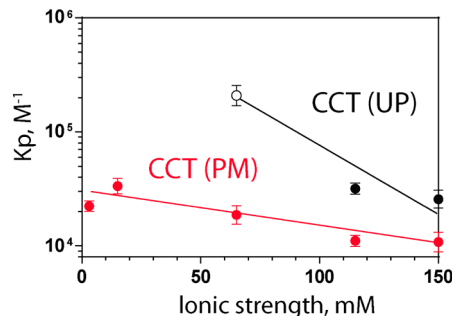


**Figure 4.** Ionic strength dependence for the binding of CCT (UP) and CCT (PM). Binding to 112 nm vesicles composed of 30 mol % PG at the indicated ionic strengths was measured by tryptophan blue-shift analysis. Each data point is the average  $K_p$  value  $\pm$  95% confidence interval for two independent experiments. The data point in the empty black circle represents a  $K_p$  value that is likely underestimated, as there was no excess lipid present at  $EC_{50}$ . Thus, the ionic strength dependence for CCT (UP) is even stronger than the graph suggests.

Information). We monitored membrane binding using the fluorescence blue-shifts of an engineered tryptophan at V37 in the middle of the m-AH (Figure 1B). The W37 peak fluorescence shifted from  $\sim 350$  nm in buffer to  $\sim 325$  nm at saturating lipid concentrations, indicating that it had relocated to the hydrophobic environment of the membrane (Figure 5A). A comparison of the binding to PG/PC SUVs of the W37 variant monitored by Trp fluorescence versus wild-type  $\alpha$ -syn via CD revealed a similar L/P ratio for half-maximal binding, within a factor of 2 (data not shown). This suggests the Trp

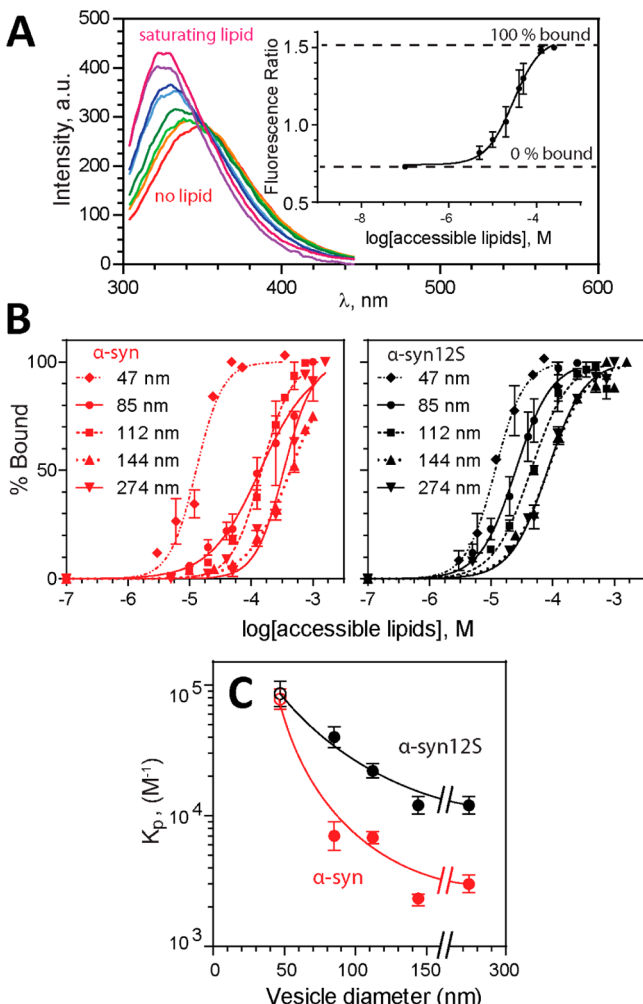


**Figure 5.** Curvature dependence of  $\alpha$ -syn and  $\alpha$ -syn12S probed by Trp fluorescence. (A) The fluorescence of tryptophan shows a blue-shift and an increase in intensity upon titration of  $\alpha$ -syn12S (1  $\mu$ M) with 85 nm LUVs (30 mol % PG, ionic strength of 115 mM). Red to fuchsia indicates a lipid/protein molar ratio from 0 to 2000. The inset shows the corresponding lipid binding curve for this spectral set and its replicate. The fluorescence ratio in the absence of lipid was set to 0% bound, and the fluorescence ratio at saturating lipid concentration was set to 100% bound. (B) Binding curves for  $\alpha$ -syn (red) and  $\alpha$ -syn12S (black). Vesicles were composed of 30 mol % PG, and the ionic strength was 115 mM. Data were fit to eq 2 using GraphPad Prism version 5.0.  $R^2$  values are listed in Table 2. (C) Neutralizing the acidic tail of  $\alpha$ -syn increases the binding strength.  $K_p$  values were determined from the binding curves in panel B.  $K_p = 1/EC_{50}$ . Each data point is the average partition coefficient ( $K_p$ )  $\pm$  95% confidence interval for two independent binding analyses. Curves are to facilitate viewing only. The data points in the empty red and black circles represent  $K_p$  values that are likely underestimated, as there was no excess lipid present at  $EC_{50}$ . See Experimental Procedures and Table 2.

substitution had little effect on partitioning. We tested binding to different sized vesicles made of 30 mol % anionic lipid, as the highly charged membrane revealed the largest effect of phosphomimicry on the curvature sensing of CCT.

Our results showed that both  $\alpha$ -syn and the  $\alpha$ -syn12S protein were curvature-sensitive under these conditions (Figure 5B,C). The  $\alpha$ -syn protein showed weak binding to larger vesicles ( $d > 85$  nm) and a  $\geq 30$ -fold improvement in binding with SUVs, a behavior that qualitatively matches the literature reports on the curvature sensitivity of  $\alpha$ -syn.<sup>46</sup>  $\alpha$ -Syn12S showed a 3–4-fold

strengthened binding to the larger, flatter vesicles ( $d \geq 85$  nm), indicating a reduced curvature dependence (Table 2). Thus, without the repulsive charges, the binding of  $\alpha$ -syn to anionic membranes is much less dependent on curvature. However, compared to that of CCT, a decrease in the negative charge flanking the m-AH in  $\alpha$ -syn had a weaker impact on curvature dependence. The relative contributions of hydrophobic and electrostatic driving forces in  $\alpha$ -syn may differ from the CCT M + P, with  $\alpha$ -syn requiring larger modulations of membrane and/or protein charge to affect curvature sensing.

## DISCUSSION

This paper presents the first explicit demonstration of the curvature sensing feature of the m-AH of CCT in comparison with that of  $\alpha$ -synuclein, a well-described curvature-sensing protein.<sup>33,46,47,69</sup> Our data support the previously introduced idea that curvature sensing by an m-AH can be modulated by changing its charge<sup>69</sup> and specifically implicate the control of curvature sensing by charge variation in disordered regions flanking the m-AH. Our results suggest a novel potential role for phosphorylation (modeled by phosphomimicry in our experiments) as an electrostatic switch to sensitize an m-AH for curvature sensing. Modulation of curvature dependence by flanking charge was influenced by the hydrophobic character of the m-AH, as shown by the somewhat different behaviors of CCT and  $\alpha$ -syn.

One caveat associated with the apparent curvature-insensitive binding of CCT (UP) (black line in Figure 3C) is that the bound m-AH can generate curved surfaces in the larger vesicles. However, there is a clear difference between CCT (UP) and CCT (PM) in the strength of binding to large vesicles, although both induce curvature upon binding.<sup>32</sup> Although binding of the unphosphorylated form will undoubtedly be promoted by lipid packing defects, its electrostatic attraction to the highly charged vesicles is so strong that an increase in curvature-induced defects would have a marginal impact. Nonetheless, this is a complicating issue that is largely neglected in previous reports on other curvature-sensing proteins, including  $\alpha$ -syn. New microscopy-based methods that can directly correlate the vesicle size and bound protein density offer a solution to this problem.<sup>7,69</sup>

**Mechanism for the Modulation of Curvature Sensing by a Change in Protein Electrostatics.** Electrostatic repulsive switches have long been recognized as a means for dampening the binding strength of membrane-binding motifs. The classic example is the binding of polybasic motifs, as in MARCKS and src kinases, which is antagonized by phosphorylation and charge neutralization at several serines within the basic peptide.<sup>63,70,71</sup> Jensen et al.<sup>69</sup> found that curvature sensing in the  $\alpha$ -syn m-AH can be affected by amino acid substitutions that alter protein charge. They suggested that curvature sensing ability is improved when the hydrophobic component of membrane binding exceeds the electrostatic contribution, and vice versa. This model was also used to explain the differential targeting of various m-AH-containing proteins to flatter plasma membranes versus highly curved organelle membranes.<sup>3</sup>

By contrast, the charge switch we have explored in CCT and  $\alpha$ -syn occurs adjacent to rather than within the m-AH. This charge switch was most prominent for the CCT m-AH. We propose that an increase in the negative charge of the CCT tail generates electrostatic repulsion with the anionic membrane surface that destabilizes m-AH formation. Antonny described

m-AH folding and intercalation into lipid bilayers as a nucleation–propagation process<sup>2</sup> in which insertion of one hydrophobic residue serves as a nucleation point for the remaining AH to fold and intercalate. Instability due to charge repulsion at the C-terminal end of the nascent m-AH may antagonize the nucleation–propagation process. Because its electrostatics are weakened, CCT (PM) is more dependent on membrane hydrophobicity and curvature.

**The Impact of a Repulsively Charged Tail on Curvature Sensitivity May Depend on the Electrostatic–Hydrophobic Balance.** Although the charge switch in the CCT tail affected curvature sensing when membrane charge was strong, it had a weaker impact on the curvature sensitivity of  $\alpha$ -synuclein. What physicochemical properties differentiate the behavior of these two m-AH motifs? The membrane binding energy is a composite of contributions from electrostatic and hydrophobic driving forces, as well as changes in membrane and protein entropy.<sup>72</sup> The electrostatic properties of the m-AH motifs in CCT and  $\alpha$ -syn are similar. They are both net positive with similar distributions of charged residues. Basic residues flank the nonpolar helical face, whereas acidic residues are mostly opposite the nonpolar face (Figure 1B). However, the hydrophobic properties are very different. The hydrophobic face of the CCT m-AH is richer in large, bulky residues such as tryptophan and phenylalanine, whereas the hydrophobic face of the  $\alpha$ -syn m-AH is enriched with smaller residues like valine and alanine (Figure 1B). The mean hydrophobicity of the nonpolar face of CCT is twice that of  $\alpha$ -syn even though the width of this face is narrower.<sup>8</sup> The curvature sensitivity of  $\alpha$ -syn has been attributed to its very weak nonpolar face,<sup>47</sup> which would require a strongly hydrophobic (curved) membrane surface to promote binding, even when the repulsive negative charges in its flanking tail have been neutralized.

**Potential Role of Acidic Tails in Targeting m-AH Segments to Curved or Flat Membranes in Cells.** There is much literature demonstrating the remarkable curvature sensing of  $\alpha$ -syn, but this is the first time a function for the highly negatively charged tail in curvature sensing has been explored. We hypothesized that one outcome of the evolution of an acidic tail is to ensure targeting to highly curved synaptic vesicles. Our results showed that neutralizing the negative charges flanking the m-AH increased the binding affinity toward all  $>50$  nm diameter vesicles, i.e., weakened curvature dependence for binding. Thus, without the charged tail,  $\alpha$ -syn would bind more strongly and with less discrimination between flat and curved organelles in the cell. This suggests that the charged tail of  $\alpha$ -syn could promote curvature sensing in cells. Without these repulsive charges, the binding of  $\alpha$ -syn to anionic membrane is much less dependent on curvature.  $\alpha$ -Synuclein can be phosphorylated at four other sites in its acidic tail, which may further decrease binding affinity and augment curvature dependence. However, reports on the membrane binding effects of phosphorylation, phosphomimicry, or tyrosine nitrosylation within the tail region of  $\alpha$ -syn are somewhat conflicting.<sup>73–75</sup>

Although CCT has been linked to curvature induction in cells,<sup>28–31,76</sup> its curvature sensing role is more tenuous. In many cells, CCT $\alpha$  is in the nucleus, where the inner nuclear membrane is a relatively flat zone rich in anionic lipids,<sup>77</sup> resulting in a scenario similar to panel C or D of Figure 3. In such cases, the strong electrostatics may drive indiscriminate membrane binding of unphosphorylated CCT $\alpha$ , but phosphor-

ylation could direct CCT away from the flatter nuclear envelope and onto the curved nucleoplasmic reticulum, which consists of tubular invaginations of the envelope.<sup>29</sup> Lastly, curvature sensing and phosphorylation could facilitate the response of CCT to biophysical properties of membranes with a PC deficiency. PC deficiency results in an increase in the density of anionic lipids and nonbilayer favoring lipids, which can augment lipid packing defects.<sup>8,13</sup> Phosphorylation might sensitize CCT to bind only to membrane regions with enhanced packing defects typified by PC deficiency.

Aside from CCT and  $\alpha$ -synuclein, there are other proteins containing m-AH motifs whose phosphorylation may modulate membrane binding and/or curvature sensing. Pah1p is a lipin that catalyzes the conversion of phosphatidate to diacylglycerol and contains an ALPS-like m-AH. Its dephosphorylation is crucial for translocation onto membranes, potentially via a membrane curvature sensing mechanism.<sup>78</sup> The membrane tether, Vps41, functions in vesicle–vacuole fusion in yeast. It contains an ALPS motif that can be phosphorylated on serines in its polar face, which weakens binding of the ALPS to the large flat vacuole membrane and allows a switch to a new protein partner and binding of Vps41 to coated vesicles.<sup>79</sup> A third example, the synaptic vesicle-clustering protein, synapsin, also binds membranes via a curvature-sensing ALPS, and its membrane binding is regulated by phosphorylation.<sup>80</sup> How phosphorylation modulates membrane binding of these proteins has not been fully explored. Our results provide a framework for exploring phosphorylation-dependent mechanisms for the control of curvature sensing in these and potentially other proteins.

## ■ ASSOCIATED CONTENT

### § Supporting Information

Effect of lipids on the secondary structure transitions of  $\alpha$ -syn12S (Figure S1). This material is available free of charge via the Internet at <http://pubs.acs.org>.

## ■ AUTHOR INFORMATION

### Corresponding Author

\*Department of Molecular Biology and Biochemistry, Simon Fraser University, Burnaby, British Columbia, Canada V5A 1S6. E-mail: cornell@sfu.ca. Telephone: (778) 782-3709. Fax: (778) 782-5583.

### Present Address

<sup>§</sup>J.M.C.L.: Department of Chemistry, University of British Columbia, Vancouver, British Columbia, Canada V6T 1Z1.

### Author Contributions

S.S.Y.C. contributed to the methods, data collection and analyses, and figure and manuscript preparation. S.G.T. contributed to research design, data analyses, and editing of the manuscript. J.M.C.L. contributed to method development as well as plasmid and protein preparation. R.B.C. contributed to the experimental design, data analyses, and manuscript preparation. The manuscript was written through contributions of all authors. All authors have given approval to the final version of the manuscript.

### Funding

This work was supported by a grant to R.B.C. from the Natural Sciences and Engineering Research Council of Canada.

### Notes

The authors declare no competing financial interests.

## ACKNOWLEDGMENTS

We thank Ziwei Ding and Jaeyong Lee for construction of several plasmids, Dr. B. Friskin, Gabriel Espinosa, and Rasoul Narimani for their assistance with DLS measurements, and Mohammad Javad Tabesh for his assistance with data collection and analysis. We thank Dr. D. Eliezer for the original  $\alpha$ -synuclein plasmid.

## ABBREVIATIONS

CCT, CTP:phosphocholine cytidylyltransferase;  $\alpha$ -syn,  $\alpha$ -synuclein; m-AH, membrane-induced amphipathic helix; PC, phosphatidylcholine; PG, phosphatidylglycerol; CD, circular dichroism; PD, Parkinson's disease; ALPS, amphipathic lipid packing sensor; UP, unphosphorylated; PM, phosphomimic;  $K_p$ , apparent partition coefficient; EC<sub>50</sub>, accessible lipid concentration at 50% bound protein.

## REFERENCES

- (1) Hu, J., Shibata, Y., Voss, C., Shemesh, T., Li, Z., Coughlin, M., Kozlov, M. M., Rapoport, T. A., and Prinz, W. A. (2008) Membrane proteins of the endoplasmic reticulum induce high-curvature tubules. *Science* 319, 1247–1250.
- (2) Antonny, B. (2011) Mechanisms of membrane curvature sensing. *Annu. Rev. Biochem.* 80, 101–123.
- (3) Bigay, J., and Antonny, B. (2012) Curvature, lipid packing, and electrostatics of membrane organelles: Defining cellular territories in determining specificity. *Dev. Cell* 23, 886–895.
- (4) Bhatia, V. K., Hatzakis, N. S., and Stamou, D. (2010) A unifying mechanism accounts for sensing of membrane curvature by BAR domains, amphipathic helices and membrane-anchored proteins. *Semin. Cell Dev. Biol.* 21, 381–390.
- (5) Cui, H., Lyman, E., and Voth, G. A. (2011) Mechanism of membrane curvature sensing by amphipathic helix containing proteins. *Biophys. J.* 100, 1271–1279.
- (6) Drin, G., and Antonny, B. (2010) Amphipathic helices and membrane curvature. *FEBS Lett.* 584, 1840–1847.
- (7) Hatzakis, N. S., Bhatia, V. K., Larsen, J., Madsen, K. L., Bolinger, P. Y., Kunding, A. H., Castillo, J., Gether, U., Hedegard, P., and Stamou, D. (2009) How curved membranes recruit amphipathic helices and protein anchoring motifs. *Nat. Chem. Biol.* 5, 835–841.
- (8) Cornell, R. B., and Taneva, S. G. (2006) Amphipathic helices as mediators of the membrane interaction of amphitropic proteins, and as modulators of bilayer physical properties. *Curr. Protein Pept. Sci.* 7, 539–552.
- (9) Vanni, S., Vamparys, L., Gautier, R., Drin, G., Etchebest, C., Fuchs, P. F., and Antonny, B. (2013) Amphipathic lipid packing sensor motifs: Probing bilayer defects with hydrophobic residues. *Biophys. J.* 104, 575–584.
- (10) Davies, S. M., Epand, R. M., Kraayenhof, R., and Cornell, R. B. (2001) Regulation of CTP:phosphocholine cytidylyltransferase activity by the physical properties of lipid membranes: An important role for stored curvature strain energy. *Biochemistry* 40, 10522–10531.
- (11) Drin, G., Casella, J. F., Gautier, R., Boehmer, T., Schwartz, T. U., and Antonny, B. (2007) A general amphipathic  $\alpha$ -helical motif for sensing membrane curvature. *Nat. Struct. Mol. Biol.* 14, 138–146.
- (12) Wiprecht, T., Beyermann, M., and Seelig, J. (2002) Thermodynamics of the coil- $\alpha$ -helix transition of amphipathic peptides in a membrane environment: The role of vesicle curvature. *Biophys. Chem.* 96, 191–201.
- (13) Vamparys, L., Gautier, R., Vanni, S., Bennett, W. F., Tielemans, D. P., Antonny, B., Etchebest, C., and Fuchs, P. F. (2013) Conical lipids in flat bilayers induce packing defects similar to that induced by positive curvature. *Biophys. J.* 104, 585–593.
- (14) Cornell, R. B., and Northwood, I. C. (2000) Regulation of CTP:phosphocholine cytidylyltransferase by amphitropism and relocalization. *Trends Biochem. Sci.* 25, 441–447.
- (15) Lee, J., Johnson, J., Ding, Z., Paetzl, M., and Cornell, R. B. (2009) Crystal structure of a mammalian CTP:phosphocholine cytidylyltransferase catalytic domain reveals novel active site residues within a highly conserved nucleotidyltransferase fold. *J. Biol. Chem.* 284, 33535–33548.
- (16) Taneva, S., Johnson, J. E., and Cornell, R. B. (2003) Lipid-induced conformational switch in the membrane binding domain of CTP:phosphocholine cytidylyltransferase: A circular dichroism study. *Biochemistry* 42, 11768–11776.
- (17) Friesen, J. A., Campbell, H. A., and Kent, C. (1999) Enzymatic and cellular characterization of a catalytic fragment of CTP:phosphocholine cytidylyltransferase  $\alpha$ . *J. Biol. Chem.* 274, 13384–13389.
- (18) Ding, Z., Taneva, S. G., Huang, H. K., Campbell, S. A., Semenec, L., Chen, N., and Cornell, R. B. (2012) A 22-mer segment in the structurally pliable regulatory domain of metazoan CTP:phosphocholine cytidylyltransferase facilitates both silencing and activating functions. *J. Biol. Chem.* 287, 38980–38991.
- (19) Huang, H. K., Taneva, S. G., Lee, J., Silva, L. P., Schriemer, D. C., and Cornell, R. B. (2013) The membrane-binding domain of an amphitropic enzyme suppresses catalysis by contact with an amphipathic helix flanking its active site. *J. Mol. Biol.* 425, 1546–1564.
- (20) Bogan, M. J., Agnes, G. R., Pio, F., and Cornell, R. B. (2005) Interdomain and membrane interactions of CTP:phosphocholine cytidylyltransferase revealed via limited proteolysis and mass spectrometry. *J. Biol. Chem.* 280, 19613–19624.
- (21) MacDonald, J. I., and Kent, C. (1994) Identification of phosphorylation sites in rat liver CTP:phosphocholine cytidylyltransferase. *J. Biol. Chem.* 269, 10529–10537.
- (22) Kent, C. (1997) CTP:phosphocholine cytidylyltransferase. *Biochim. Biophys. Acta* 1348, 79–90.
- (23) Wang, Y., and Kent, C. (1995) Effects of altered phosphorylation sites on the properties of CTP:phosphocholine cytidylyltransferase. *J. Biol. Chem.* 270, 17843–17849.
- (24) Watkins, J. D., and Kent, C. (1991) Regulation of CTP:phosphocholine cytidylyltransferase activity and subcellular location by phosphorylation in Chinese hamster ovary cells. The effect of phospholipase C treatment. *J. Biol. Chem.* 266, 21113–21117.
- (25) Hatch, G. M., Jamil, H., Utal, A. K., and Vance, D. E. (1992) On the mechanism of the okadaic acid-induced inhibition of phosphatidylcholine biosynthesis in isolated rat hepatocytes. *J. Biol. Chem.* 267, 15751–15758.
- (26) Arnold, R. S., DePaoli-Roach, A. A., and Cornell, R. B. (1997) Binding of CTP:phosphocholine cytidylyltransferase to lipid vesicles: Diacylglycerol and enzyme dephosphorylation increase the affinity for negatively charged membranes. *Biochemistry* 36, 6149–6156.
- (27) Dennis, M. K., Taneva, S. G., and Cornell, R. B. (2011) The intrinsically disordered nuclear localization signal and phosphorylation segments distinguish the membrane affinity of two cytidylyltransferase isoforms. *J. Biol. Chem.* 286, 12349–12360.
- (28) Goulbourne, C. N., Malhas, A. N., and Vaux, D. J. (2011) The induction of a nucleoplasmic reticulum by prelamin A accumulation requires CTP:phosphocholine cytidylyltransferase- $\alpha$ . *J. Cell Sci.* 124, 4253–4266.
- (29) Malhas, A., Goulbourne, C., and Vaux, D. J. (2011) The nucleoplasmic reticulum: Form and function. *Trends Cell Biol.* 21, 362–373.
- (30) Gehrig, K., Cornell, R. B., and Ridgway, N. D. (2008) Expansion of the nucleoplasmic reticulum requires the coordinated activity of lamins and CTP:phosphocholine cytidylyltransferase  $\alpha$ . *Mol. Biol. Cell* 19, 237–247.
- (31) Lagace, T. A., and Ridgway, N. D. (2005) The rate-limiting enzyme in phosphatidylcholine synthesis regulates proliferation of the nucleoplasmic reticulum. *Mol. Biol. Cell* 16, 1120–1130.
- (32) Taneva, S. G., Lee, J. M., and Cornell, R. B. (2012) The amphipathic helix of an enzyme that regulates phosphatidylcholine synthesis remodels membranes into highly curved nanotubules. *Biochim. Biophys. Acta* 1818, 1173–1186.
- (33) Kahle, P. J., Neumann, M., Ozmen, L., Muller, V., Jacobsen, H., Schindzielorz, A., Okochi, M., Leimer, U., van Der Putten, H., Probst,

A., Kremmer, E., Kretzschmar, H. A., and Haass, C. (2000) Subcellular localization of wild-type and Parkinson's disease-associated mutant  $\alpha$ -synuclein in human and transgenic mouse brain. *J. Neurosci.* 20, 6365–6373.

(34) Burre, J., Sharma, M., Tsetsenis, T., Buchman, V., Etherton, M. R., and Sudhof, T. C. (2010)  $\alpha$ -Synuclein promotes SNARE-complex assembly in vivo and in vitro. *Science* 329, 1663–1667.

(35) Auluck, P. K., Caraveo, G., and Lindquist, S. (2010)  $\alpha$ -Synuclein: Membrane interactions and toxicity in Parkinson's disease. *Annu. Rev. Cell Dev. Biol.* 26, 211–233.

(36) Conway, K. A., Harper, J. D., and Lansbury, P. T. (1998) Accelerated in vitro fibril formation by a mutant  $\alpha$ -synuclein linked to early-onset Parkinson disease. *Nat. Med.* 4, 1318–1320.

(37) Fink, A. L. (2006) The aggregation and fibrillation of  $\alpha$ -synuclein. *Acc. Chem. Res.* 39, 628–634.

(38) Volles, M. J., and Lansbury, P. T., Jr. (2003) Zeroing in on the pathogenic form of  $\alpha$ -synuclein and its mechanism of neurotoxicity in Parkinson's disease. *Biochemistry* 42, 7871–7878.

(39) Periquet, M., Fulga, T., Myllykangas, L., Schlossmacher, M. G., and Feany, M. B. (2007) Aggregated  $\alpha$ -synuclein mediates dopaminergic neurotoxicity in vivo. *J. Neurosci.* 27, 3338–3346.

(40) Jao, C. C., Hegde, B. G., Chen, K., Haworth, I. S., and Langen, R. (2008) Structure of membrane-bound  $\alpha$ -synuclein from site-directed spin labeling and computational refinement. *Proc. Natl. Acad. Sci. U.S.A.* 105, 19666–19671.

(41) Bussell, R., Jr., and Eliezer, D. (2003) A structural and functional role for 11-mer repeats in  $\alpha$ -synuclein and other exchangeable lipid binding proteins. *J. Mol. Biol.* 329, 763–778.

(42) Davidson, W. S., Jonas, A., Clayton, D. F., and George, J. M. (1998) Stabilization of  $\alpha$ -synuclein secondary structure upon binding to synthetic membranes. *J. Biol. Chem.* 273, 9443–9449.

(43) Nuscher, B., Kamp, F., Mehnert, T., Odo, S., Haass, C., Kahle, P. J., and Beyer, K. (2004)  $\alpha$ -Synuclein has a high affinity for packing defects in a bilayer membrane: A thermodynamics study. *J. Biol. Chem.* 279, 21966–21975.

(44) Recchia, A., Debetto, P., Negro, A., Guidolin, D., Skaper, S. D., and Giusti, P. (2004)  $\alpha$ -Synuclein and Parkinson's disease. *FASEB J.* 18, 617–626.

(45) Eliezer, D. (2013) The mysterious C-terminal tail of  $\alpha$ -synuclein: Nanobody's guess. *J. Mol. Biol.* 425, 2393–2396.

(46) Middleton, E. R., and Rhoades, E. (2010) Effects of curvature and composition on  $\alpha$ -synuclein binding to lipid vesicles. *Biophys. J.* 99, 2279–2288.

(47) Pranke, I. M., Morello, V., Bigay, J., Gibson, K., Verbavatz, J. M., Antonny, B., and Jackson, C. L. (2011)  $\alpha$ -Synuclein and ALPS motifs are membrane curvature sensors whose contrasting chemistry mediates selective vesicle binding. *J. Cell Biol.* 194, 89–103.

(48) Kjaer, L., Giehm, L., Heimburg, T., and Otzen, D. (2009) The influence of vesicle size and composition on  $\alpha$ -synuclein structure and stability. *Biophys. J.* 96, 2857–2870.

(49) Ouberai, M. M., Wang, J., Swann, M. J., Galvagnion, C., Williams, T., Dobson, C. M., and Welland, M. E. (2013)  $\alpha$ -Synuclein senses lipid packing defects and induces lateral expansion of lipids leading to membrane remodeling. *J. Biol. Chem.* 288, 20883–20895.

(50) Varkey, J., Isas, J. M., Mizuno, N., Jensen, M. B., Bhatia, V. K., Jao, C. C., Petrlova, J., Voss, J. C., Stamou, D. G., Steven, A. C., and Langen, R. (2010) Membrane curvature induction and tubulation are common features of synucleins and apolipoproteins. *J. Biol. Chem.* 285, 32486–32493.

(51) Bisaglia, M., Tessari, I., Pinato, L., Bellanda, M., Giraudo, S., Fasano, M., Bergantino, E., Bubacco, L., and Mammi, S. (2005) A Topological Model of the Interaction between  $\alpha$ -Synuclein and Sodium Dodecyl Sulfate Micelles. *Biochemistry* 44, 329–339.

(52) Drescher, M., Veldhuis, G., van Rooijen, B. D., Milikisants, S., Subramaniam, V., and Huber, M. (2008) Antiparallel Arrangement of the Helices of Vesicle-Bound  $\alpha$ -Synuclein. *J. Am. Chem. Soc.* 130, 7796–7797.

(53) Georgieva, E. R., Ramlall, T. F., Borbat, P. P., Freed, J. H., and Eliezer, D. (2010) The lipid-binding domain of wild type and mutant  $\alpha$ -synuclein: Compactness and interconversion between the broken and extended helix forms. *J. Biol. Chem.* 285, 28261–28274.

(54) Bartlett, G. R. (1959) Phosphorus assay in column chromatography. *J. Biol. Chem.* 234, 466–468.

(55) Bradford, M. M. (1976) A rapid and sensitive method for the quantitation of microgram quantities of protein utilizing the principle of protein-dye binding. *Anal. Biochem.* 72, 248–254.

(56) Cornell, R. B. (1991) Regulation of CTP:phosphocholine cytidylyltransferase by lipids. 1. Negative surface charge dependence for activation. *Biochemistry* 30, 5873–5880.

(57) Taneva, S. G., Patty, P. J., Friskin, B. J., and Cornell, R. B. (2005) CTP:phosphocholine cytidylyltransferase binds anionic phospholipid vesicles in a cross-bridging mode. *Biochemistry* 44, 9382–9393.

(58) Brewer, J. M., Tetley, L., Richmond, J., Liew, F. Y., and Alexander, J. (1998) Lipid vesicle size determines the Th1 or Th2 response to entrapped antigen. *J. Immunol.* 161, 4000–4007.

(59) Frederick, T. E., Chebukati, J. N., Mair, C. E., Goff, P. C., and Fanucci, G. E. (2009) Bis(monoacylglycerol)phosphate forms stable small lamellar vesicle structures: Insights into vesicular body formation in endosomes. *Biophys. J.* 96, 1847–1855.

(60) Matsuzaki, K., Murase, O., Sugishita, K., Yoneyama, S., Akada, K., Ueha, M., Nakamura, A., and Kobayashi, S. (2000) Optical characterization of liposomes by right angle light scattering and turbidity measurement. *Biochim. Biophys. Acta* 1467, 219–226.

(61) Mayer, L. D., Hope, M. J., and Cullis, P. R. (1986) Vesicles of variable sizes produced by a rapid extrusion procedure. *Biochim. Biophys. Acta* 858, 161–168.

(62) Sreerama, N., and Woody, R. W. (2000) Estimation of protein secondary structure from circular dichroism spectra: Comparison of CONTIN, SELCON, and CDSSTR methods with an expanded reference set. *Anal. Biochem.* 287, 252–260.

(63) Murray, D., Hermida-Matsumoto, L., Buser, C. A., Tsang, J., Sigal, C. T., Ben-Tal, N., Honig, B., Resh, M. D., and McLaughlin, S. (1998) Electrostatics and the membrane association of Src: Theory and experiment. *Biochemistry* 37, 2145–2159.

(64) Buser, C. A., and McLaughlin, S. (1998) Ultracentrifugation technique for measuring the binding of peptides and proteins to sucrose-loaded phospholipid vesicles. *Methods Mol. Biol.* 84, 267–281.

(65) Mesmin, B., Drin, G., Levi, S., Rawet, M., Cassel, D., Bigay, J., and Antonny, B. (2007) Two lipid-packing sensor motifs contribute to the sensitivity of ArfGAP1 to membrane curvature. *Biochemistry* 46, 1779–1790.

(66) Dowhan, W. (1997) Molecular basis for membrane phospholipid diversity: Why are there so many lipids? *Annu. Rev. Biochem.* 66, 199–232.

(67) Lim, L., and Wenk, M. R. (2009) Neuronal Membrane Lipids: Their Role in the Synaptic Vesicle Cycle. In *Neural Lipids* (Tettamanti, G., and Goracci, G., Eds.) pp 224–238, Springer Science.

(68) Shai, Y. (1999) Mechanism of the binding, insertion and destabilization of phospholipid bilayer membranes by  $\alpha$ -helical antimicrobial and cell non-selective membrane-lytic peptides. *Biochim. Biophys. Acta* 1462, 55–70.

(69) Jensen, M. B., Bhatia, V. K., Jao, C. C., Rasmussen, J. E., Pedersen, S. L., Jensen, K. J., Langen, R., and Stamou, D. (2011) Membrane curvature sensing by amphipathic helices: A single liposome study using  $\alpha$ -synuclein and annexin B12. *J. Biol. Chem.* 286, 42603–42614.

(70) McLaughlin, S., and Aderem, A. (1995) The myristoyl-electrostatic switch: A modulator of reversible protein-membrane interactions. *Trends Biochem. Sci.* 20, 272–276.

(71) McLaughlin, S., and Murray, D. (2005) Plasma membrane phosphoinositide organization by protein electrostatics. *Nature* 438, 605–611.

(72) Tamm, L. K. (1994) Physical Studies of Peptide–Bilayer Interactions. In *Membrane Protein Structure* (White, S. H., Ed.) pp 283–313, Springer, New York.

(73) Kuwahara, T., Tonegawa, R., Ito, G., Mitani, S., and Iwatsubo, T. (2012) Phosphorylation of  $\alpha$ -synuclein protein at Ser-129 reduces

neuronal dysfunction by lowering its membrane binding property in *Caenorhabditis elegans*. *J. Biol. Chem.* 287, 7098–7109.

(74) Visanji, N. P., Wislet-Gendebien, S., Oschipok, L. W., Zhang, G., Aubert, I., Fraser, P. E., and Tandon, A. (2011) Effect of Ser-129 phosphorylation on interaction of  $\alpha$ -synuclein with synaptic and cellular membranes. *J. Biol. Chem.* 286, 35863–35873.

(75) Sevcik, E., Trexler, A. J., Dunn, J. M., and Rhoades, E. (2011) Allostery in a disordered protein: Oxidative modifications to  $\alpha$ -synuclein act distally to regulate membrane binding. *J. Am. Chem. Soc.* 133, 7152–7158.

(76) Gehrig, K., and Ridgway, N. D. (2011) CTP:phosphocholine cytidylyltransferase  $\alpha$  (CCT $\alpha$ ) and lamins alter nuclear membrane structure without affecting phosphatidylcholine synthesis. *Biochim. Biophys. Acta* 1811, 377–385.

(77) Garnier-Lhomme, M., Byrne, R. D., Hobday, T. M., Gschmeissner, S., Woscholski, R., Poccia, D. L., Dufourc, E. J., and Larijani, B. (2009) Nuclear envelope remnants: Fluid membranes enriched in sterols and polyphosphoinositides. *PLoS One* 4, e4255.

(78) Karanasios, E., Han, G. S., Xu, Z., Carman, G. M., and Siniossoglou, S. (2010) A phosphorylation-regulated amphipathic helix controls the membrane translocation and function of the yeast phosphatidate phosphatase. *Proc. Natl. Acad. Sci. U.S.A.* 107, 17539–17544.

(79) Cabrera, M., Langemeyer, L., Mari, M., Rethmeier, R., Orban, I., Perz, A., Brocker, C., Griffith, J., Klose, D., Steinhoff, H. J., Reggiori, F., Engelbrecht-Vandre, S., and Ungermann, C. (2010) Phosphorylation of a membrane curvature-sensing motif switches function of the HOPS subunit Vps41 in membrane tethering. *J. Cell Biol.* 191, 845–859.

(80) Krabben, L., Fassio, A., Bhatia, V. K., Pechstein, A., Onofri, F., Fadda, M., Messa, M., Rao, Y., Shupliakov, O., Stamou, D., Benfenati, F., and Haucke, V. (2011) Synapsin I senses membrane curvature by an amphipathic lipid packing sensor motif. *J. Neurosci.* 31, 18149–18154.